Regular Article

ANALYTICAL
AND BIOANALYTICAL
CHEMISTRY
RESEARCH

Published by the
Iranian Chemical Society

***Anal. Bioanal. Chem. Res.**, Vol. 11, No. 3, 335-342, July 2024.*

Development of a Low-Cost Microfluidic Kit for the Smartphone-Based Colorimetric Determination of As(III) in Drinking Water Samples

Bahareh Moradifar[a], Abbas Afkhami[a,b,*], Tayyebeh Madrakian[a], Sina Khalili[a] and Mohammad Reza Jalali Sarvestani[a]

[a]*Department of Analytical Chemistry, Faculty of Chemistry and Petroleum Sciences, Bu-Ali Sina University, Hamedan, 6517838695, Iran*

[b]*D-8 International University, Hamedan, Iran*

(Received 28 March 2024, Accepted 19 April 2024)

As(III) determination is of great importance in various industries such as environmental monitoring, pharmaceuticals, and metallurgy. In this respect, a nanocomposite of sucrose-modified gold nanoparticles (Au@Suc) was synthesized and characterized by UV-visible spectrophotometry and transmission electron microscopy (TEM) methods. Then, the applicability of the synthesized nanocomposite for the development of a microfluidic kit for the colorimetric point-of-care (POC) detection of As(III) ions was scrutinized. The experimental parameters for the microfluidic kit were optimized using the one-factor-at-a-time (OFAT) approach. The effective conditions for the microfluidic kit were found to be a flow rate of 0.15 ml min^{-1}, a path length of 5.50 cm, and a pH of 7.0. The resulting microfluidic kit indicated a direct correlation between the red component of RGB pixels in images captured by a smartphone and the concentration of As(III) ions in the range of 0.09-1.20 µM, with a detection limit of 0.054 µM. Evaluation of the microfluidic kit's selectivity revealed no significant interference. Additionally, the microfluidic kit was successfully employed to analyze As(III) in various drinking water samples, with recovery values ranging between 95.01% and 105.00%.

Keywords: As(III), Microfluidic, Colorimetry, Au nanoparticle, Smartphone

INTRODUCTION

Arsenic is a naturally occurring element found in soil, water, and air. Exposure to arsenic can occur through various means including drinking contaminated water, consuming contaminated food, or inhaling contaminated air [1]. Arsenic exposure can also occur in occupational settings such as mining, smelting, and pesticide applications. As(III) is one of the most common oxidation states of arsenic [2]. As(III) toxicity has been linked to various health problems and diseases, making it a significant public health concern [3]. The health effects of As(III) toxicity can range from acute symptoms to long-term health issues [4]. Acute symptoms of arsenic poisoning can include vomiting, abdominal pain, diarrhea, and even death in severe cases. Long-term exposure to arsenic can lead to skin lesions, increased risk of cancer (including skin, bladder, and lung cancer), cardiovascular disease, and diabetes [5]. In addition, arsenic exposure has been linked to developmental effects in children and reproductive problems in adults [6]. Therefore, trace quantities of As(III) determination is of great importance. Several techniques are available for determining the presence of As(III) in various samples, including hydride generation atomic absorption spectrometry (HGAAS) [7], hydride generation inductively coupled plasma mass spectrometry (HG-ICP-MS) [8], X-ray fluorescence (XRF) spectrometry [9], and ion chromatography (IC) [10]. The aforementioned analytical methods pose several drawbacks, including high costs in equipment purchase and maintenance, complex operations requiring specialized expertise, extensive sample

*Corresponding author. E-mail: Afkhami@basu.ac.ir

preparation, sensitivity to environmental conditions and interferences, and complex data interpretation [11].

Microfluidic-based analytical devices have revolutionized the field of analytical chemistry, offering numerous advantages over traditional techniques [12]. These devices enable precise manipulation of small volumes of fluids, leading to reduced reagent consumption and waste generation. This is particularly beneficial for expensive or limited-quantity reagents and applications requiring high-throughput screening [13]. The miniaturization of the analytical system allows for rapid mixing and reaction kinetics, resulting in faster analysis times and improved sensitivity [14]. Additionally, the small footprint of microfluidic devices makes them ideal for portable or point-of-care applications, eliminating the need for complex and bulky instrumentation [15]. Furthermore, the integration of multiple analytical functions within a single microfluidic platform offers the potential for automated and multiplexed analysis, reducing the need for manual intervention and increasing experimental throughput [16,17]. Lastly, the precise control of fluid flow and chemical gradients within microfluidic channels enables the development of novel analytical techniques and assays that are not feasible with conventional methods [18]. In conclusion, microfluidic-based analytical devices have the potential to significantly advance the field of analytical chemistry by offering enhanced precision, reduced waste, faster analysis times, and the development of novel analytical techniques [19]. The employment of smartphone-based image analysis utilizing the RGB (Red, Green, Blue) color model has gained remarkable traction across various sectors including healthcare, agriculture, and environmental monitoring [20]. This technology facilitates swift and non-intrusive assessment of diverse parameters by examining the color composition of images captured by smartphone cameras [21]. The RGB color model is based on the additive color theory, wherein varying intensities of red, green, and blue light are combined to generate a wide spectrum of colors [22]. The application of smartphone-based image analysis employing the RGB color model has the capacity to reform various sectors by providing cost-effective, non-intrusive, and easily accessible solutions for data gathering and analysis [23]. This technology can democratize access to crucial information and insights, particularly in resource-limited settings where traditional analytical methods may be impractical or excessively costly [24]. As smartphone technology advances, one can anticipate further progress in the realm of smartphone-based image analysis employing the RGB color model. These advancements are likely to uncover fresh applications and avenues for innovation, impacting fields from medical diagnostics to precision agriculture and beyond [25]. A novel microfluidic system was developed to detect As(III) ions in water using color changes of sucrose-coated Au nanoparticles. The system was optimized to ensure the highest sensitivity. Testing in drinking water samples showed its potential to improve As(III) monitoring, offering valuable water safety and quality control.

MATERIALS AND METHODS

Chemicals and Apparatus

The investigation made use of chemicals and reagents sourced from respected suppliers including Sigma-Aldrich and Merck (Darmstadt, Germany), and did not require additional purification. The microfluidic chip design was developed using Solid Works 2022 software and then printed onto a polymethyl methacrylate (PMMA) support using a CO_2 laser instrument RT6090 from Rotec, Iran. For injections and fluid circulation within the system, a labv3 peristaltic pump from Senchen company was utilized. The pH of solutions was determined using an 827 Metrohm pH meter, and a Samsung A22 smartphone was used as the detector, with the RGB color detector application employed for image analysis. Furthermore, absorbance measurements were carried out using a WPA UV-visible spectrophotometer. Transmission Electron Microscopy (TEM) images were captured using a S208 EPM instrument. In preparation for the experiments, a stock solution of As_2O_3 at a concentration of 2×10^{-3} M was prepared by initially dissolving the powder in HCl 0.1 M and then adjusting the pH to 7.0 with a concentrated solution of NaOH. Fresh solutions were prepared daily from this stock solution. All solutions were prepared using doubly distilled water (DDW) to ensure the purity of the experimental setup.

Synthesis of Au Nanoparticles Modified with Sucrose (Au@Suc)

Synthesis of gold nanoparticles was performed from the

reduction of gold ions in $HAuCl_4$ aqueous solution with sodium borohydride reducing reagent ($NaBH_4$) and sucrose stabilization agent. For the synthesis,12 5 µl of aqueous solution of $HAuCl_4$ 10 g l^{-1} in volume 12.5 ml (0.095 g l^{-1}) was placed in water and ice bath at 4 °C and stirred for 5 min. Then, 500 µl of 2.5% sucrose was slowly added to it, and finally, after 5 min, 125 µl of 2.5% $NaBH_4$ solution containing 2.5% sucrose was added to the solution as a droplet and very slowly. Then, the resulting nanocomposite Au@Suc composite was separated from the solution using centrifugation at 4000 rpm for a duration of 15 min. The separated composite was then carefully dried at room temperature.

PMMA Microfluidic Kit Design and Fabrication

The process of fabricating the microfluidic kit began with the initial design of the mold using SolidWorks 2022 software. This design was then translated into a physical form by printing it onto a PMMA support using a CO_2 laser instrument RT6090 from Rotec, Iran. The resulting model, as depicted in Fig. 1, served as the foundation for the fabrication process. Subsequently, two additional PMMA layers were carefully positioned on the top and beneath the main microfluidic kit, as illustrated in Fig. 1S. This multi-layered approach was essential for ensuring the structural integrity and functionality of the final product. To further secure the layers and prevent any potential leakage during the fabrication process, the entire assembly was inserted into an oven set at 300 °C. This heating process not only facilitated the bonding of the layers but also served to eliminate any residual stresses within the material, thereby enhancing the overall robustness of the microfluidic kit.

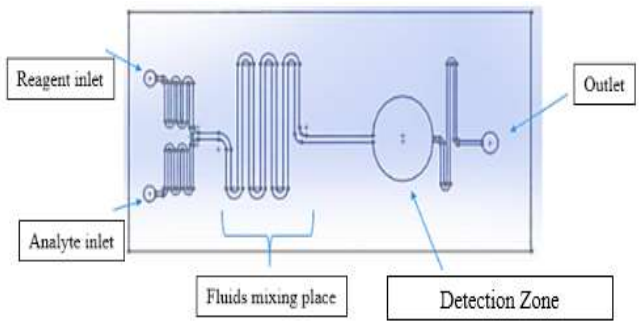

Fig. 1. The sketch of the designed microfluidic kit.

Experimental Procedure

The microfluidic kit was meticulously placed inside a light-tight cubic chamber, as depicted in Fig. 2S, to ensure that the smartphone camera had a designated space, minimizing any potential interference from ambient light on the analytical response. Subsequently, the hoses were securely connected to the valves of the microfluidic kit, and (DDW) was systematically pumped into the system using a peristaltic pump to confirm the absence of any leaks. Following this, 0.5 ml of the analyte, with varying concentrations, and nanocomposite solutions (prepared under optimal conditions including a flow rate of 0.15 ml min^{-1}, a path length of 5.50 cm, and a pH of 7.0) were introduced into the chip. Once the two solutions had been thoroughly mixed within the reaction chamber/detector section of the chip, imaging was conducted, and the RGB values for the resulting solution were duly recorded.

RESULTS AND DISCUSSION

Characterization of Au@Suc

The TEM images of the Au@Suc nanocomposite show that the particles are spherical and well-dispersed, with an average size of 25 nm. When As(III) ions are introduced, significant aggregation occurs, causing color changes in the solution. This aggregation may result from interactions between the As(III) ions and the particle surface, leading to changes in optical properties. The alterations in color play a crucial role in the analysis of As(III) ion detection, allowing for both qualitative and quantitative assessments. Consequently, the TEM images not only yield significant information regarding the structure and dispersion of the nanocomposite particles but also visually elucidate the mechanism involved in detecting As(III) ions [26]. The UV-visible spectra in Fig. 3A display the Au@Suc nanocomposite without As(III) ions, while Fig. 3B shows the spectra with their presence [26]. The spectra indicate that the peak wavelength (λ_{max}) of the Au@Suc nanocomposite is 530 nm. Upon the addition of As(III) ions, there is a marginal decrease in this peak, and a new peak emerges at 680 nm [26]. The changes observed in the localized surface plasmon resonance (LSPR) properties of the Au@Suc nanocomposite indicate a significant alteration. The decrease in the peak at 530 nm suggests a reduction in the collective oscillation of

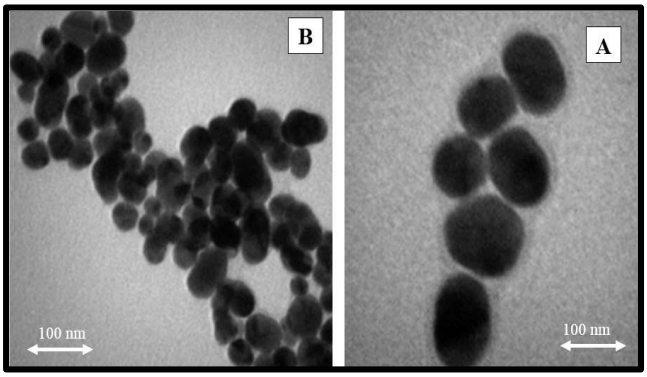

Fig. 2. TEM images of Au@Suc in the absence of As(III) (A), in the presence of As(III) [0.13 M] (B).

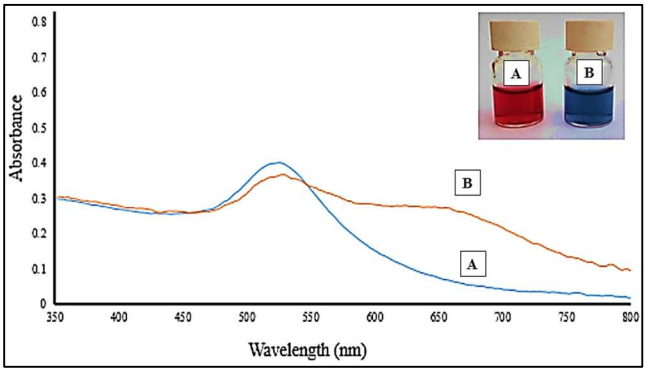

Fig. 3. The UV-visible spectra of Au@Suc in the absence of As(III) (A), in the presence of As(III) [0.13 µM] (B).

free electrons in the conduction band of the nanoparticles. Additionally, the appearance of a new peak at 680 nm is linked to the aggregation of nanoparticles in the presence of As(III) ions. These findings point to a noteworthy shift in the behavior of the nanocomposite, highlighting the impact of As(III) ions on nanoparticle aggregation and LSPR properties.

Optimization of Effective Experimental Factors and Analytical Parameters

The analytical response, ΔS_B, was calculated using the following equation.

$$\Delta S_B = S_{B,\ As(III)\ solution} - S_{B,\ blank}$$

The S_B value represents the blue component of the calculated RGB value for each image analyzed by the smartphone. The selection of the blue pigment was based on its high sensitivity and selectivity, as depicted in Fig. 3. Upon the addition of As(III) to the Au@Suc solution, a visible color change from red to blue occurred, discernible to the naked eye. To fine-tune the experimental parameters, including solution pH, path length, and flow rate, a one-factor-at-a-time (OFAT) approach was utilized to achieve optimal sensitivity. We initially focused on optimizing the solution pH. Several solutions containing 0.75 µM As(III) at varying pH levels were prepared, and their analytical response (ΔS_B) was measured. The results revealed that the maximum response was attained at pH 7.0. It seems that under more acidic conditions, the protonation of sucrose hinders the interaction of As(III) with the nanocomposite, whereas in more alkaline conditions, the formation of oxyanions of As(III) disrupts the interactions [26]. For optimizing the factor of path length, several microfluidic kits were designed with varying lengths from 2.0 to 9.0 cm. The analytical response of each kit was measured, and the results are shown in Fig. 4B. It was observed that as the path length increased from 2.0 to 5.5 cm, the analytical response also increased sharply, after which it remained constant. This indicates that the kinetic of As(III) reaction with the nanocomposite is relatively slow, and in path lengths shorter than 5.5 cm, the reaction cannot be completed. Therefore, 5.5 cm was determined to be the optimum path length [26]. The final optimized parameter was the flow rate, and to evaluate this parameter, a 0.75 µM solution of As(III) was passed through a microfluidic kit with a 5.5 cm path length at different flow rates ranging from 0.01 to 0.25. The results of this evaluation are presented in Fig. 4C. Based on the provided data, it is evident that the ΔS_B increases as the flow rate is raised from 0.01 to 0.15 ml min^{-1}, followed by a slight decrease. It appears that at low flow rates, the formation of air bubbles impacts the analytical response of the system, while at flow rates higher than 0.15 ml min^{-1}, there is insufficient time for the complete reaction of As(III) with the nanocomposite [26]. Consequently, 0.15 ml min^{-1} has been identified as the optimal flow rate.

The graph in Fig. 4D shows the strong correlation between As(III) concentration and signal change (ΔS_B) within the range of 0.09-1.20 µM. A slope of 12.46 indicates the change in signal with respect to As(III) concentration,

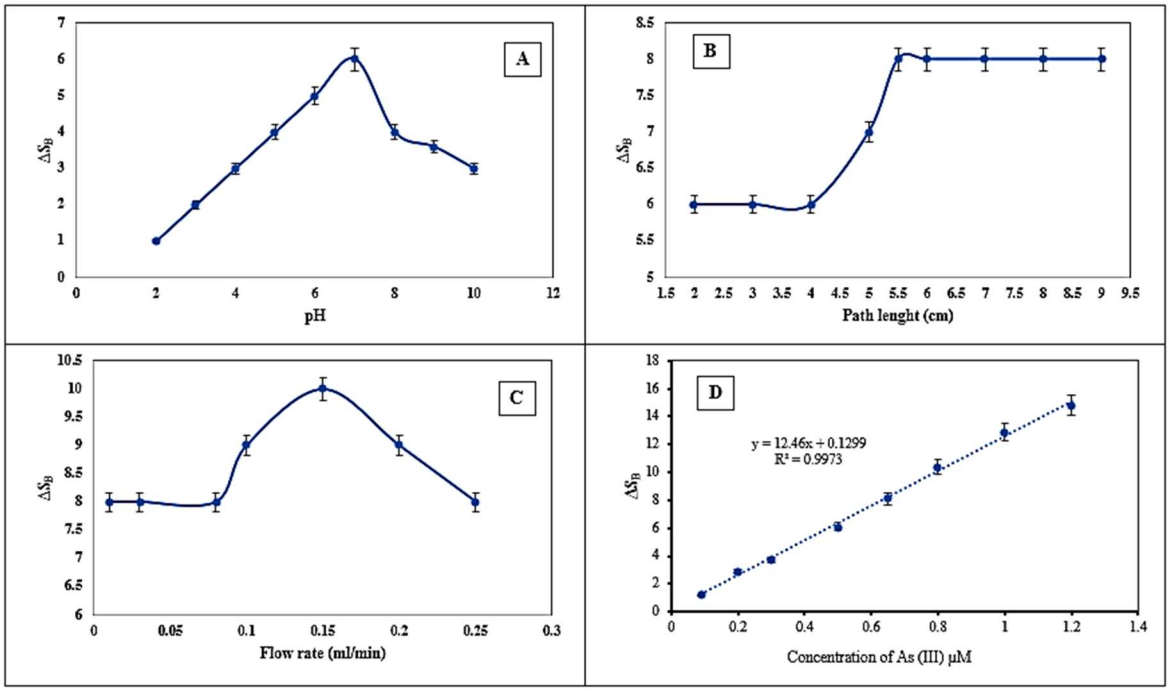

Fig. 4. Optimization of pH in 4 cm path length and 0.1 ml min^{-1} flow rate(A), Path length in pH = 7.0 and 0.1 ml min^{-1} flow rate (B), Flow rate in pH = 7.0 and 5.5 cm path lenght (C) for a 0.75 µM solution of As(III) and the resulting calibration curve at the optimium conditions (D).

while the y-intercept of 0.1299 represents ΔS_B at zero As(III) concentration. The high correlation coefficient (0.9973) confirms the reliable linear relationship, demonstrating the accuracy of the method within this range. The detection limit was also calculated by IUPAC recommended $3S_D/M$ approach and the obtained value was 0.054 µM.

Selectivity and Reproducibility

The proposed method's selectivity was thoroughly tested by creating a 1 µM solution of As(III) and introducing various quantities of different cations and anions to the solution. The objective was to compute ΔS_B for each solution and identify the level of interfering species that could result in a fluctuation in the analytical response (ΔS_B) of ≥5%, which was considered the tolerance limit [27]. The selectivity of the suggested method over 22 ionic species was analyzed, and the outcomes are outlined in Table 1. The analysis indicated that the developed method demonstrates outstanding selectivity towards As(III). To further assess the reliability of the proposed method, repeatability and reproducibility were also examined. For repeatability testing, five distinct solutions of As(III) with a concentration of 1 µM were prepared, and their ΔS_B was measured using a single microfluidic kit. The %RSD was subsequently calculated and found to be 2.28%, indicating good repeatability of the method. Additionally, the reproducibility of the designed method was assessed by creating a 1 µM solution of As(III) and measuring its ΔS_B in five different microfluidic kits. The %RSD for reproducibility was determined to be 4.18%, further demonstrating the robustness of the method.

Real Sample Analysis

The microfluidic kit designed for the determination of As(III) was successfully tested using five different drinking water samples collected from various areas in Hamedan, Iran. The samples were spiked with three different concentrations of As(III) ions and analyzed using the proposed method. The results, presented in Table 2, showed Recovery values ranging from 95.01% to 105.00% and RSD values below 5.34%. These findings indicate that the developed method

Table 1. Interference of some Foreign Species for a 1 μM Solution of As(III)

Interfering species	Tolerance limit
Hg^{2+}, Ni^{2+}, Mg^{2+}, Cl^{-}, SO_4^{2-}	1000
Pb^{2+}, Cr^{3+}, K^{+}, Na^{+}, NH_4^{+}, Sb^{2+}	
CO_3^{2-}, PO_4^{3-}, NO_3^{-}, NO_2^{--} Cd^{2+}, Cu^{2+}, Co^{2+}, As(V), Ca^{2+}	800
Fe^{3+}, Zn^{2+}	500

Table 2. The Real Sample Analysis Results

Samples	Added amounts (μM)	Found amounts (μM)	RSD (%, n = 3)	Recovery (%)
	0.000	ND*	-	-
Drinking water 1	0.100	0.098	3.31	98.0
	0.400	0.410	1.53	102.5
	0.600	0.630	0.54	105.0
	0.000	ND*	-	-
Drinking water 2	0.100	0.10	4.74	100.0
	0.400	0.410	3.13	102.5
	0.600	0.630	1.76	105.0
	0.000	ND*	-	-
Drinking water 3	0.100	0.100	3.95	100.0
	0.400	0.380	2.22	95.0
	0.600	0.620	0.78	103.3
	0.000	0.080	4.85	-
Drinking water 4	0.100	0.103	4.43	103.0
	0.400	0.475	2.81	98.8
	0.600	0.630	1.65	105.0
	0.000	0.100	5.34	-
Drinking water 5	0.100	0.200	5.01	100.0
	0.400	0.490	3.71	97.5
	0.600	0.620	2.42	103.3

*Not detected.

has good reproducibility and acceptable accuracy, validating its potential for practical use in analyzing As(III) levels in drinking water [28,29].

Comparison of the Proposed Technique with Former Analytical Methods

The analytical techniques previously used to determine As(III) have been complex and involved expensive instrumentation, time-consuming sample preparation, and the need for experienced operators. These methods provided high sensitivity and low detection limits, but their drawbacks included tedious sample preparation steps and the requirement for skilled personnel to carry out the analysis. However, the microfluidic kit developed in this research offers a more straightforward approach for the determination of As(III) compared to conventional techniques. The

advantages of the microfluidic kit include simplicity, portability, low-cost instrumentation, very high selectivity, and short analysis time. This innovative approach addresses the limitations of previous methods and provides a more efficient and accessible solution for the determination of As(III).

CONCLUSION

The study describes the synthesis and characterization of a sucrose-modified Au (Au@Suc) nanocomposite using UV-visible spectrophotometry and transmission electron microscopy (TEM). The nanocomposite was then utilized in the development of a microfluidic kit for the colorimetric point of care (POC) detection of As(III) ions. The experimental parameters for the microfluidic kit were optimized using one factor at the time (OFAT) method. The optimal conditions for the microfluidic kit were found to be a flow rate of 0.15 ml min^{-1}, a path length of 5.50 cm, and a pH of 7.0. The developed microfluidic kit showed a linear relationship between the red component of RGB pixels in images captured by a smartphone and the concentration of As(III) ions in the range of 0.09-1.20 µM. The method's detection limit was determined to be 0.054 µM. The microfluidic kit's selectivity was evaluated, and no significant interference was observed. Additionally, the suitability of the microfluidic kit for determining As(III) in various drinking water samples was successfully demonstrated, with recovery values falling within the range of 95.01-105.00%. In conclusion, the study presents a novel approach for the colorimetric detection of As(III) ions using a microfluidic kit based on a sucrose-modified Au nanocomposite, with potential applications in point-of-care testing and environmental monitoring.

REFERENCES

[1] M. Bissen, F.H. Frimmel, Acta Hydrochim. Hydrobiol. 31 (2003) 9.
[2] Jomova, Klaudia, Z. Jenisova, M. Feszterova, S. Baros, J. Liska, D. Hudecova, Chistopher J. Rhodes, M. Valko, J. Appl. Toxicol. 31 (2011) 95.
[3] M.F. Hughes, Toxicol. Lett. 133 (2002) 1.
[4] K.J. Rader, P.M. Dombrowski, K.J. Farley, J.D. Mahony, D.M. Di Toro, Environ. Toxicol. Chem. 23 (2004) 1649.
[5] J. Gailer, Biochimie. 91 (2009) 1268.
[6] P. Finnegan, W. Chen, Front. Physiol. 3 (2012) 24498.
[7] B.E. dos Santos Costa, N.M. Melo Coelho, J. Food. Compos. Anal. 95 (2021) 103686.
[8] Z. Chen, B. Chen, M. He, B. Hu, Microchim. Acta 187 (2020) 1.
[9] S. Majumder, E. Marguí, G. Roman-Ross, D. Chatterjee, M. Hidalgo, Talanta 217 (2020) 121005.
[10] Y. Lin, Y. Sun, X. Wang, S. Chen, Y. Wu, F. Fu Fu, Microchem. J. 159 (2020) 105592.
[11] C.Y. Hou, L.M. Fu, W.J. Ju, P.Y. Wu, Chem. Eng. J. 398 (2020) 125573.
[12] X. Jing, H. Wang, X. Huang, Z. Chen, J. Zhu, X. Wang, Food. Chem. 337 (2021) 127971.
[13] H. Shi, S. Jiang, B. Liu, Z. Liu, N.M. Reis, Microchem. J. 171 (2021) 106845.
[14] C.J.D. Laurenciano, C.C. Tseng, S.J. Chen, S.Y. Lu, L.L. Tayo, L.M. Fu, Talanta 231 (2021) 122362.
[15] T. Thongkam, K. Hemavibool, Microchem. J. 159 (2020) 105412.
[16] A.C.R. Sousa, C.N. Makara, L.C. Brazaca, E. Carrilho, Food. Chem. 356 (2021) 129692.
[17] J. Aksorn, S. Teepoo, Talanta 207 (2020) 120302.
[18] V.A.O.P. da Silva, R.C. Freitas, P. R. Oliveira, R.C. Moreira, L.H. Marcolino-Junior, M.F. Bergamini, W.K.T. Coltro, B.C. Janegitz, Measurement 164 (2020) 108085.
[19] Y. Fan, J. Li, Y. Guo, L. Xie, G. Zhang, Measurement 171 (2021) 108829.
[20] T.T. Wang, C.K. Lio, H. Huang, R.Y. Wang, H. Zhou, P. Luo, L.S. Qing, Talanta 206 (2020) 120211.
[21] S. Balbach, N. Jiang, R. Moreddu, X. Dong, W. Kurz, C. Wang, J. Dong, Anal. Methods 13 (2021) 4361.
[22] G.M. Fernandes, R.S. Weida, D.N. Barreto, R.S. Lamarca, P. C.F. Lima Gomes, J.F. da S Petruci, A.D. Batista, Anal. Chim. Acta 1135 (2020) 187.
[23] F.C. Böck, G.A. Helfer, A. Ben da Costa, M.B. Dessuy, M.F. Ferrão, J. Chemom. 34 (2020) e3251.
[24] S. Qian, Y. Cui, Z. Cai, L. Li, Biosens. Bioelectron. X 11 (2022) 100173.
[25] T. Alawsi, G.P. Mattia, Z. Al-Bawi, R. Beraldi, Sens. Bio-Sens. Res. 32 (2021) 100404.

[26] K. Shrivas, S. Patel, D. Sinha, S.S. Thakur, T.K. Patle, T. Kant, K. Dewangan, M.L. Satnami, J. Nirmalkar, S. Kumar, Microchim. Acta 187 (2020) 1.

[27] A. Motalebizadeh, H. Bagheri, S. Asiaei, N. Fekrat, A. Afkhami, RSC. Adv. 8 (2018) 27091.

[28] S. Ebrahimi, A. Afkhami, T. Madrakian, Z. Amouzegar, Electrochim. Acta. 437 (2023) 141496.

[29] A. Afkhami, T. Madrakian, A. Afshar Assl, Talanta 55 (2001) 55.